Chance is an important element in phagolysosomal acidification that favors the macrophage

Quigly Dragotakes[1], Kaitlin Stouffer[1], Man Shun Fu[1], Carlos M. De Leon-Rodriguez[1], Joudeh B. Freij[1], Aviv Bergman[2], Arturo Casadevall[1]

[1]Department of Molecular Microbiology and Immunology, Johns Hopkins School of Public Health, Baltimore, MD and [2]Department of Systems and Computational Biology, Albert Einstein College of Medicine, Bronx, NY.

Running title: Chance contributes to host defense

Address correspondence

Arturo Casadevall MD, PhD

Johns Hopkins School of Public Health

615 N. Wolfe Street

Room E5132

Baltimore, Maryland 21205

Abstract

Phagosome acidification is a critical mechanism of defense in phagocytic cells, which inhibits microbes by producing a less hospitable pH that also activates microbicidal mechanisms. We analyzed the dynamic distribution of phagolysosome pH measurements after bone marrow derived macrophages had ingested live *Cryptococcus neoformans* or *C. gattii* cells, dead *C. neoformans* cells, or inert beads at various time intervals. Phagosomes acidified for each type of ingested particle, producing a range of pH values that approximated normal distributions, yet the degree to which they differed from normality depended on the particle type. Irrespective of the particle ingested, we noted wide variation in the phagolysosomal pH measured. Analysis of the increment of pH reduction revealed no forbidden ordinal pH intervals for each type of particle indicative of chaotic signatures; consistent with the notion that the phagosomal acidification process is a result of a stochastic dynamical system. The stochastic nature of phagosomal acidification is consistent with the fact that final vacuolar pH is the result of numerous variables that contribute to the final outcome, which was also reflected in a stochastic initiation of intracellular cell budding. Hence, "chance" plays an important role in the process of phagosomal acidification which, in turn, introduces unpredictability to the outcome of the macrophage-microbe struggle in individual phagosomes thus creating a fundamental uncertainty in the fate of host-microbe interactions. Chance provides macrophages with an adaptive bet hedging strategy that can increase the likelihood that phagolysosomal pH inhibits ingested microbes while reducing the emergence of acid resistance.

Introduction

Audaces fortuna iuvat (Fortune favors the bold) - Virgil

Phagocytosis is a fundamental cellular process used by unicellular organisms for nutrient acquisition as well as by host immune cells for capturing and killing microbial cells. The parallels between food acquisition and immunity have led to the suggestion that these two processes had a common evolutionary origin [1]. The process of phagocytosis results in the formation of a phagosome, a dynamic membrane bounded organelle, which represents a critical location in the struggle between the host and microbial cells [2]. Microbial ingestion into phagosomes results in exposure to host cell microbicidal mechanisms, which for some microbes leads to death while others survive by subverting critical aspects of phagosome maturation and by damaging phagosome structural integrity.

Phagosomal formation can be followed by a process of maturation whereby the multimeric protein complex vacuolar (V) V-ATPase is added to the phagosomal membrane, then pumps protons into the lumen of the mature phagosome or phagolysosome using cytosolic ATP for energy (reviewed in [2]). Proton pumping into phagolysosomal lumen results in acidification, which inhibits and kills many ingested microorganisms. Consequently, some types of microbes, such as *Mycobacterium tuberculosis* and *Histoplasma capsulatum*, interfere with phagosomal maturation and acidification to promote their intracellular survival. The extent of phagosomal acidification is determined by numerous mechanisms that include the proton flux through the pump, proton consumption in the phagosomal lumen, and backflow into the cytoplasm [3]. Phagosome acidification in macrophage is rapid with pH of 6 being reached within 10 min after ingestion [4] and 5.4 by 15-20 min [5].

Cryptococcus neoformans is a facultative intracellular pathogen [6]. Upon ingestion by macrophages *C. neoformans* resides in a mature acidic phagosome [7]. The outcome of macrophage-*C. neoformans* interaction is highly variable depending on whether the fungal cell is killed, inhibited, or not. If not

killed, *C. neoformans* can replicate intracellularly resulting in variable outcomes that include death and lysis of the host cell, non-lytic exocytosis [8, 9], transfer to another macrophage [10, 11], or phagosomal persistence. A critical variable in determining the outcome of the *C. neoformans*-macrophage interaction is the integrity of the phagosomal membrane, with maintenance of this barrier conducive to control of intracellular infection while loss of integrity leads to host cell death [12].

Prior studies of *C. neoformans* phagosomal acidification have shown great variation in phagolysosomal pH [12-14]. The cryptococcal phagolysosomal pH is affected by several microbial variables that include urease expression [13], phagosomal membrane integrity [12], and the presence of the cryptococcal capsule with its glucuronic acid residues that can influence final pH through their acid base properties [15]. *C. neoformans* capsule size increases intracellularly as part of a stress response which can potentially affect the phagolysosomal pH through increasing the phagosome volume, thus diluting its contents and promoting membrane damage through physical stress [12]. In this study, we analyzed the distribution of phagolysosomal pHs in murine macrophages as a dynamical system and find that it is stochastic in nature. Our results imply that the usage of chance is an important strategy in phagosomal acidification, which may echo through the immune process to introduce a fundamental uncertainty in the outcome of microbe-macrophage interactions.

Methods

Phagolysosomal pH measurement. Phagolysosomal pH was measured using ratiometric fluorescence imaging involving the use of pH-sensitive probe Oregon green 488 as described in prior studies [13]. The pH values analyzed here were collected in part during prior studies of *C. neoformans*-macrophage interactions [12-14]. Briefly, Oregon green 488 was first conjugated to monoclonal antibody (mAb) 18B7, which binds *C. neoformans* capsular polysaccharide, using Oregon Green 488 Protein Labeling Kit

(Molecular Probes, Eugene, OR). The labeling procedure was done by following the manufacture's instruction. Bone marrow derived macrophages (BMDM) were plated at a density of 1.25×10^5 cells/well on 24-well plate with 12 mm circular coverslip. Cells were cultured in Dulbecco's Modified Eagle Medium (DMEM) with 20 % L-929 cell-conditioned medium, 10 % FBS (Atlanta Biologicals, Flowery Branch, GA), 2mM Glutamax (Gibco, Gaithersburg MD), 1 % nonessential amino acid (Cellgro, Manassas, VA), 1 % HEPES buffer (Corning, Corning, NY), 1 % penicillin-streptomycin (Corning), 0.1 % 2-mercaptoethanol (Gibco),and activated with 0.5 µg/ml lipopolysaccharide (LPS; Sigma-Aldrich) and 100 U/ml interferon gamma (IFN-γ; Roche),at 37 °C in a 9.5 % CO_2 atmosphere overnight. Prior to infection, live, heat killed H99, R265, WM179, ure1, or cap59 strain or anti-mouse IgG coated polystyrene bead (3.75×10^6 cells or beads/ml) were incubated with 10 µg/ml Oregon green conjugated mAb 18B7 for 15 min. Macrophages were then incubated with Oregon green conjugated mAb 18B7-opsonized particles in 3.75×10^5 cryptococcal cells or beads per well. Cells were centrifuged immediately at 350 x g for 1 min and culture were incubated at 37 °C for 10 min to allow phagocytosis. Extracellular cryptococcal cells or beads were removed by washing three times with fresh medium, a step that prevents the occurrence of new phagocytic events. Samples on coverslip were collected at their respective time points after phagocytosis by washing twice with pre-warmed HBSS and placing upside down on MatTek petri dish (MatTek, Ashland, MA) with HBSS in the microwell. Images were taken by using Olympus AX70 microscopy (Olympus, Center Valley, PA) with objective 40x at dual excitation 440 nm and 488 nm, and emission 520 nm. Images were analyzed using MetaFluor Fluorescence Ratio Imaging Software (Molecular Devices, Downingtown, PA). Fluorescence intensities were used to determine the ratios of Ex488 nm/Ex440 nm that were converted to absolute pH values using a standard curve where the images are taken as above but intracellular pH of macrophages was equilibrated by adding 10 µM nigericin in pH buffer (140 mM KCl, 1 mM $MgCl_2$, 1 mM $CaCl_2$, 5 mM glucose, and appropriate buffer ≤

pH 5.0: acetate-acetic acid; pH 5.5-6.5: MES; ≥ pH 7.0: HEPES. Desired pH values were adjusted using either 1 M KOH or 1 M HCl). The pH of buffers was adjusted at3-7 using 0.5-pH unit increments.

Time-lapse imaging and intracellular replication. The time of intracellular replication here were collected in time-lapse imaging during prior studies of *C. neoformans*-macrophage interactions [13]. For imaging BMDM (5×10^4 cells/well) were plated on poly-D-lysine coated coverslip bottom MatTek petri dishes with 14mm microwell (MatTek). Cells were cultured in completed DMEM medium and stimulated with 0.5 µg/ml LPS and 100 U/ml IFN-γ overnight at 37 °C with 9.5 % CO_2. On the following day, macrophages were infected with cryptococcal cells (H99 or ure1; 1.5×10^5 cells/well) opsonized with 18B7 (10 µg/ml). After 2 h incubation to allow phagocytosis, extracellular cryptococcal cells were removed by washing the culture five times with fresh medium. Images were taken every 4 min for 24 h using a Zeiss Axiovert 200M inverted microscope with a 10x phase objective in an enclosed chamber at 9.5 % CO_2 and 37 °C. The time intervals to initial replication of individual cryptococcal cells inside macrophage were measured in time-lapse imaging.

Data Processing. Phagolysosome pH intervals were calculated by subtracting measured pH levels of phagolysosomes from a starting pH of 7.2, and individual interval measurements were concatenated into a single dataset for each time point examined.

Data analysis. Discrimination of deterministic vs. stochastic dynamics was achieved using the previously characterized permutation spectrum test [16]. In this method, the processed datasets were segmented into overlapping subsets of 4 data points using a sliding window approach, as detailed in figure 4, and assigned 1 of 24 (4!) possible ordinal patterns based on the ordering of the 4 terms in the subset. The frequencies with which each unique ordinal pattern occurred in the dataset were then calculated and plotted. Deterministic dynamics were characterized by the occurrence of "forbidden ordinals", equal to ordinal patterns that occurred with a frequency of 0 in the dataset whereas stochastic dynamics were

characterized by the absence of any forbidden ordinals. Further characterization of deterministic dynamics was achieved using the previously characterized point count plot [17], in which periodic vs. chaotic dynamics were differentiated based on the distribution of "peaks" in the calculated power spectrum of each dataset. Power spectrums were estimated with Matlab's Lomb-Scargle power spectral density (PSD) estimate function and subsequently normalized. From the normalized power spectrum, "point count plots" were generated by counting the number of peaks above a set threshold—the point threshold—with values of the point threshold ranging from 0 to 1. Periodic dynamics were characterized by "staircase" point count plots whereas chaotic dynamics were characterized by point count plots with a decreasing exponential shape.

Distribution and normality analysis. Each set of sample data was fit to a series of distributions using the R package "fitdistrplus" with default parameters for each distribution type, generating the histograms and Quantile-Quantile (Q-Q) plots. Normality and significance was calculated via the base R Shapiro-Wilk test [18].

Results

During studies of phagosome acidification after the ingestion of *C. neoformans* by murine macrophages we noted a wide distribution in pH of the resulting phagolysosomes. Given that growth rate of *C. neoformans* is highly affected by pH [13, 19] and that the outcome of the *C. neoformans*-macrophage interaction is likely to be determined in the phagosome [12, 20, 21], we decided to analyze the distribution of phagolysosomal pH mathematically to gain insight into the dynamics of this process. A scheme of the method used to determine phagosomal acidification with representative data from polystyrene bead phagocytosis experiments is shown in Figure 1.

Figure 1. pH measurement of phagolysosome. (A) Ratiometric measuring scheme where macrophages ingested either polystyrene beads coated with anti-mouse IgG or cryptococcal cells. Opsonization was antibody-mediated using monoclonal IgG 18B7 conjugated to the pH sensitive probe Oregon green. Phagolysosomal pH was measured by using dual-excitation ratio fluorescence imaging. (B) Representative radiometric images of phagolysosomal-containing beads. Images were taken while intracellular pH of macrophages was equilibrated in buffer clamped at various pH values (pH 3.5-6.5). MetaMorph software was used to generate a ratiometric image where pH is represented by a color. Scale bar, 10 µm. (C) Representative standard curve of mean fluorescence excitation ratio (488 nm excitation/440 nm excitation: 520 nm emission) of Oregon green bead-loaded macrophages with phagolysosomes equalized in calibration buffers at pH 3.5 to 6.5. (D) Representative images of beads inside macrophage taken at 440 nm excitation (Ex440), 488 nm excitation (Ex488), bright field (BF), and pseudo color images of the 488ex/440ex ratio with pH color scale displayed at the right panels. Scale bar, 10 µm. (E) Violin plot with dots representing pH of individual phagolysosomes-containing beads.

Phagolysosomal pH are normally distributed. We analyzed 3057, 4023, 437, and 499 individual phagolysosomal pH measurements after bone marrow derived macrophages had ingested live *C. neoformans* or *C. gattii* cells, dead *C. neoformans* cells, or inert beads at various time intervals, respectively. To determine whether phagolysosome pH measurements followed a normal distribution, the measured relative pH values were fit to a normal distribution using the "fitdistrplus" R statistical package. We found that across all time intervals and for each of the four types of samples, phagolysosome pH measurements approximated a normal distribution (Figure 2 and 3, SFigures 1-5). Q-Q plots for all samples and conditions yielded mostly straight lines in the region of the average pH although most distributions showed skewing away from a normal distribution at the extreme higher and lower pHs.

Figure 2. Raw phagolysosomal pH data fit to normal distribution for polystyrene beads. Data from each sample was graphed as a frequency density histogram (left) and Q-Q plot (right) according to a normal distribution. Theoretical normal distribution overlays the density histogram as a red solid line. This sample deviated from a normal distribution ($p < 9.18E-01$, 2.26E-01, 6.54E-03, and 6.31E-01 for 1, 2, 3, and 4 h time intervals, respectively).

Figure 3. Raw phagolysosomal pH data fit to normal distribution for strain H99. Data from each sample was graphed as a frequency density histogram (left) and Q-Q plot (right) according to a normal distribution. Theoretical normal distribution overlays the density histogram as a red solid line. This sample deviated from a normal distribution ($p < 2.73E-05$, 3.49E-10, 2.00E-06, 7.75E-14, 8.88E-09, and 8.96E-36 for 0, 1, 2, 3, 4, and 24 h time intervals, respectively).

Supplemental Figure 1. Raw phagolysosomal pH data fit to normal distribution for strain R265. Data from each sample was graphed as a frequency density histogram (left) and Q-Q plot (right) according to a normal distribution. Theoretical normal distribution overlays the density histogram as a red solid line. This sample deviated from a normal distribution ($p < 3.81E-11$, 2.88E-06, 4.61E-06, 5.31E-04, 2.09E-09, and 7.06E-18 for 0, 1, 2, 3, 4, and 24 h timepoints, respectively).

Supplemental Figure 2. Raw phagolysosomal pH data fit to normal distribution for strain W179. Data from each sample was graphed as a frequency density histogram (left) and Q-Q plot (right) according to a normal distribution. Theoretical normal distribution overlays the density histogram as a red solid line. This sample deviated from a normal distribution ($p < 4.80E-13$, 4.34E-18, 5.72E-12, 1.52E-05, 4.94E-05, and 3.01E-03 for 0, 1, 2, 3, 4, and 24 h timepoints, respectively).

Supplemental Figure 3. Raw phagolysosomal pH data fit to normal distribution for strain ure1. Data from each sample was graphed as a frequency density histogram (left) and Q-Q plot (right) according to a normal distribution. Theoretical normal distribution overlays the density histogram as a red solid line.

198 This sample deviated from a normal distribution ($p < 1.56E-09$, 1.79E-06, 3.03E-11, and 1.11E-02 for 1, 2,
199 3, and 4 h timepoints, respectively).

200 **Supplemental Figure 4.** Raw phagolysosomal pH data fit to normal distribution for strain cap59. Data
201 from each sample was graphed as a frequency density histogram (left) and Q-Q plot (right) according to
202 a normal distribution. Theoretical normal distribution overlays the density histogram as a red solid line.
203 This sample deviated from a normal distribution ($p < 6.12E-27$).

204 **Supplemental Figure 5.** Raw phagolysosomal pH data fit to normal distribution for heat killed strain H99.
205 Data from each sample was graphed as a frequency density histogram (left) and Q-Q plot (right)
206 according to a normal distribution. Theoretical normal distribution overlays the density histogram as a
207 red solid line. This sample deviated from a normal distribution ($p < 4.67E-13$, 4.27E-05, 3.26E-01, and
208 1.62E-02 for 1, 2, 3, and 4 h timepoints, respectively).

209 Live *C. neoformans* skew phagolysosomal pH away from a normal distribution. We evaluated the
210 normality of the phagolysosome pH populations as a function of time by visualization of the data
211 overlaid with a normal curve, Q-Q plots (Figures 2 and 3, SFigure 1-5), and via the Shapiro-Wilk test
212 (Table I, Figure 4), an established statistical test of normality as a function of distance between observed
213 and expected measurements in relation to their order statistics [18]. The pH of phagolysosomes
214 containing ingested beads met Shapiro-Wilk criteria for a normal distribution for measurements at three
215 of four intervals, as we were unable to reject the null hypothesis ($p > 0.05$). In contrast, the distributions
216 of phagolysosomal pH containing live and dead yeast cells at various time intervals each manifested
217 significant deviations from normality. The closest distribution of phagolysosomal pHs with yeast
218 particles that met Shapiro-Wilk criteria for normality was for ingested heat-killed *C. neoformans* at 3 h
219 post infection. We found no consistent pattern between strains of cryptococcal species with C.
220 neoformans strain H99 decreasing, C. gattii strain R265 increasing then decreasing, and *C. gattii* strain

WM179 only increasing in normality of the dataset. Both bead and ure1 mutant ingested phagolysosomes displayed no clear trend, and heat killed ingested phagolysosomes displayed a sharp increase followed by tapering. The degree of normality for distributions of phagolysosomal pHs for phagolysosomes containing live cells varied significantly among strains and times and none meet Shapiro-Wilk criteria for a normal distribution at any time. Visualization of each dataset's respective Q-Q plot affirmed these trends, with the least amounts of skewing in bead ingested phagolysosomes or heat-killed ingested phagolysosomes at 3 h post infection.

Table I. Shapiro-Wilk p values for each sample at each timepoint for which data was acquired.

	Beads	**H99**	**R265**	**WM179**	**ure1**	**cap59**	**Heat Killed**
0 h		2.73E-05	3.81E-11	4.80E-13			
1 h	9.18E-01	3.49E-10	2.88E-06	4.34E-18	1.56E-09		4.67E-13
2 h	2.26E-01	2.00E-06	4.61E-06	5.72E-12	1.79E-06		4.27E-05
3 h	3.26E-01	7.75E-14	5.31E-04	1.52E-05	3.03E-11		3.26E-01
4 h	6.31E-01	8.88E-09	2.09E-09	4.94E-05	1.11E-02		1.62E-02
24 h		8.96E-36	7.06E-18	3.01E-03		6.12E-27	

Table I. Normality test p values. Deviation from a normal distribution was calculated for each sample according to Shapiro-Wilk test.

Figure 4. Visualizations of normality and sample size through time. Normality measurements (line and dot) were calculated via Shapiro-Wilk testing with psi (ψ) denoting samples for which we were unable to reject the null hypothesis that these samples could come from a normal distribution ($p > 0.05$). Phagosome sample sizes (bars) indicate how many individual phagosomes were measured for each sample at each timepoint. Cap59 was omitted as only a single timepoint of data was collected.

Phagosome acidification intervals are stochastic. To determine whether phagolysosomal acidification is a deterministic or stochastic process we employed a permutation spectrum test [16] in which the distribution of ordinal patterns occurring in subsets of our full dataset were analyzed. Measured phagolysosomal pHs were subtracted from an initial pH value (7.2) based on cell media pH and placed in a vector. Subsets of 4 data points were generated using a sliding window approach in which the first four values were grouped, the window shifted by one, and the subsequent set of 4 values grouped (Figure 5). Each subset was prescribed an "ordinal pattern" based on the relative values of the data points in the subset to each other with, for instance, the lowest value assigned a "0" in the ordinal pattern and the highest a "3". The distribution of ordinal patterns across all of the subsets generated was analyzed for the existence of "forbidden patterns"—ordinal patterns that did not occur in any of the subsets. We found no forbidden patterns at any time evaluated for any of the live, dead, or bead samples (Figure 6 and 7, SFigure 6-10). The lack of forbidden patterns suggest pH acidification is a stochastic process.

Figure 5. Diagram of ordinal pattern generation using sliding window approach, as detailed by Kulp et. Al (1). A window of four terms is shifted along the entire vector of measured pH intervals. At each window position the four values are numbered from least to greatest, generating the ordinal pattern, and the resulting distribution of ordinal patterns present in the vector is analyzed. A stochastic process would result in every combination of orders being observed at a non-zero frequency. In contrast, a deterministic process would result in patterns forbidden by the underlying governing functions of this process. (A) Example of shifting window analysis. Measurements are aligned in a single vector with a scanning window of four measurements. Each value in the window is assigned a number 0-3 according to its value (least to greatest) resulting in an ordinal pattern. The ordinal patterns of every window are then analyzed for frequency. (B) An example of scanning window analysis using data from one of the *C. neoformans* experiments to better visualize the analysis.

Figure 6. Analysis of deterministic properties for polystyrene beads. Raw interval data (top), ordinal pattern analysis (middle), and point count analysis (bottom) for macrophage phagolysosome pH at 1, 2, 3, and 4 h.

Figure 7. Analysis of deterministic properties for strain H99. Raw interval data (top), ordinal pattern analysis (middle), and point count analysis (bottom) for macrophage phagolysosome pH at 0, 1, 2, 3, 4, and 24 h.

Supplemental Figure 6. Analysis of deterministic properties for strain R265. Raw interval data (top), ordinal pattern analysis (middle), and point count analysis (bottom) for macrophage phagolysosome pH at 0, 1, 2, 3, 4, and 24 h.

Supplemental Figure 7. Analysis of deterministic properties for strain WM179. Raw interval data (top), ordinal pattern analysis (middle), and point count analysis (bottom) for macrophage phagolysosome pH at 0, 1, 2, 3, 4, and 24 h.

Supplemental Figure 8. Analysis of deterministic properties for strain ure1. Raw interval data (top), ordinal pattern analysis (middle), and point count analysis (bottom) for macrophage phagolysosome pH at 1, 2, 3, and 4 h.

Supplemental Figure 9. Analysis of deterministic properties for strain cap59. Raw interval data (top), ordinal pattern analysis (middle), and point count analysis (bottom) for macrophage phagolysosome pH at 24 h.

Supplemental Figure 10. Analysis of deterministic properties for heat killed strain H99. Raw interval data (top), ordinal pattern analysis (middle), and point count analysis (bottom) for macrophage phagolysosome pH at 1, 2, 3, and 4 h.

Time intervals from ingestion of *C. neoformans* to initial budding are stochastic. *C. neoformans* replication rate is highly dependent on pH [13]. Consequently, we hypothesized that if phagolysosomal acidification followed stochastic dynamics, this would be reflected on the time interval to initial replication. Analysis of time to initial fungal cell budding revealed stochastic dynamics with no evidence of forbidden ordinal patterns (Figure 8). Similar results were observed for initial budding of wild type and urease negative strains of C. neoformans, which reside in phagolysosomes that differ in final pH as a result of ammonia generation from urea hydrolysis. Hence, for both strains the distribution was stochastic despite the fact that phagosomes of urease deficient strains are approximately 0.5 pH units lower than those of wild type strains [13].

Figure 8. Analysis of deterministic properties for intracellular replication intervals of strains (A) H99 and (B) ure1. Raw interval data (top), ordinal point analysis (middle), and point count analysis (bottom) for intervals, in minutes, between budding times.

Macrophage phagolysosomes acidify to a pH below optimal growth for soil microbes. The pH of soils varies greatly from acidic to alkaline based on variety of conditions that in turn determine the associated microbiome [22]. Since the phagolysosome is an acidic environment, we reasoned that microbes that thrived in acidic soils could provide proxy of the types of microbes that macrophages could encounter, and which pose a threat to the cell/host due to their acidophilic nature. Hence, we compared the distribution of phagolysosomal pH values obtained with latex beads as a measure of the types of acidities generated in the absence of microbial modulation relative to published soil microbe growth data as a function of pH (Figure 9). The latex bead pH distribution is narrow and centered at a pH of about 4.5, which corresponds to a pH that significantly reduces the optimal growth even for microbes in acidic soils.

Figure 9. Comparison of pH distribution for phagolysosomes containing inert polystyrene beads to the growth of soil microbes at different pH as indicated by thymidine incorporation. The frequency density of measured latex bead pH values is represented by a light blue fill. The points for the growth of soil microbes at different pHs (red dots) are averages replotted from three published experiments found in Figures 2 of [23] and 4 of [24] with error bars representing standard deviation.

Discussion

The process of phagosomal maturation encompassed by the fusion of the phagosome with lysosomes, which leads to lumen acidification, is a complex choreography that includes the recruitment of V-ATPase from lysosomes to the phagosome [25] and a large number of other protein components [26]. The complexity and sequential nature of the maturation process combined with the potential for variability at each of the maturation steps, and the noisy nature of the signaling networks that regulate this process, have led to the proposal that each phagolysosome is a unique and individual unit [27]. In fact, the action of kinesin and dynein motors that move the phagosome along microtubules has been shown to exhibit stochastic behavior adding an additional source of randomness to the process [28]. Hence, even when the ingested particle is a latex bead taken through one specific type of phagocytic receptor there is heterogeneity in phagosome composition, even within a single cell [27]. Since the phagosome is a killing machine used to control ingested microbes this heterogeneity implies there will be differences in the microbicidal efficacy of individual phagosomes. This variability raises fundamental questions about the nature of the dynamical system embodied in the process of phagosomal maturation.

In this study, we analyzed the dynamics of phagosome variability, as reflected by their pH, as a function of time for live and dead cells as well as latex particles. We aimed to characterize the dynamics as either stochastic—an inherently unpredictable process with identical starting conditions yielding different

trajectories in time vs. deterministic—a theoretically predictable process with identical starting conditions leading to identical trajectories. In particular, we focused our analysis on differentiating stochastic vs. chaotic signatures in the trajectories of phagolysosomal pH. While both dynamics might yield highly divergent trajectories for similar starting conditions (i.e. only one of 100 variables differing by only a minuscule amount), a chaotic system is inherently deterministic whereby if identical starting conditions could be replicated, the same trajectory would follow from those conditions each time. A chaotic system is defined as one so sensitive to initial conditions, however, that in practice, initial conditions cannot be replicated precisely enough to see these same trajectories follow.

Irrespective of the nature of the particle used, we observed that the distribution of the increment of phagolysosomal pH reduction was random, indicative of a stochastic process. We found no evidence that phagosome acidification was a chaotic process. Given the complexity of phagosomal maturation, and that in the case of *C. neoformans* the final pH is affected by such microbial variables as the presence of urease [13], size and composition of the capsule [6], the acid-base properties of the capsule [15], fungal cell interference with phagosome maturation [20, 29, 30], and the possibility of leakage of cytoplasmic contents as a result of membrane damage [12, 31], it is clear that a large number of variables contribute to phagosomal maturation. Systems where a large number of variables each contribute to an outcome tend to exhibit 'noise', which in turn gives them the characteristics of a stochastic dynamical system. In this regard, our finding that phagolysosomal pH demonstrates stochastic features is consistent with our current understanding of the mechanisms involved.

For *C. neoformans* there is increasing evidence that the fate of the microbe-macrophage interaction is determined by the integrity of the phagolysosomal membrane [12, 21]. For most microbes, maintenance of an acidic environment in the phagolysosome is critically determinant on the integrity of the phagolysosomal membrane to keep protons in the phagolysosomal lumen and exclude more alkaline cytoplasmic contents. For example, with *C. albicans* rupture of the phagolysosomal membrane is

350 followed by rapid alkalization of the phagolysosomal lumen [32]. For *C. neoformans*, phagolysosomal
351 integrity is compromised by secretion of phospholipases that damage membranes and the physical
352 stress on membranes resulting from capsular enlargement in the phagolysosome [12]. However, for *C.*
353 *neoformans*, loss of phagolysosomal membrane integrity does not immediately result in loss of
354 phagolysosomal acidity [12], which is attributed to buffering by glucuronic acid residues in capsule [15].
355 Adding to the complexity of the *C. neoformans*-macrophage interaction is that the phagolysosomal pH in
356 the vicinity of 5.5 matches the optimal replication pH for this fungus [13], which can be expected to
357 place additional stress on the organelle through the increased volume of budding cells. Treating
358 macrophages with chloroquine, which increases phagosomal pH [33], potentiates macrophage
359 antifungal activity against *C. neoformans* [34]. Hence, phagosomal acidification does not inhibit *C.*
360 *neoformans* replication but it is critical for activation of mechanisms involved in antigen presentation
361 [30]. In the Cryptococcal-containing phagolysosome the luminal pH is likely to also reflect a variety of
362 microbial-mediated variables which include ammonia generation from urease, capsular composition,
363 and the integrity of the phagolysosomal membrane.

364 Quantile-Quantile (Q-Q) plots revealed that most phagolysosomal pH distributions in this study
365 manifested significant deviations from normality in several instances. The most normally distributed pH
366 sets were those resulting from the ingestion of latex beads, particles that cannot modify the acidity of
367 the phagosome through capsular acid-base properties or by damaging the phagolysosomal membrane
368 and allowing contact with cytoplasmic contents. We note that for the three *C. gattii* strains the pH
369 distributions revealed more skewing in Q-Q plots than for the H99 *C. neoformans* strain. Although the
370 cause of this variation is not understood and the sample size is too small to draw firm conclusions, we
371 note that such variation could reflect more microbial-mediated modification of the phagolysosomal pH
372 by the *C. gattii* strains. In this regard, the capsular polysaccharide of *C. gattii* strains has polysaccharide
373 triads that are more complex [35] and, given that the cryptococcal polysaccharide capsule contains

374 glucuronic acids that can modify phagolysosomal pH through its acid-base properties, it is possible that
375 this skewing reflects differences in phagosome to phagosome capsular effects.

376 Analysis of the normality of phagolysosomal pH distributions as a function of time by the Shapiro-Wilk
377 test produced additional insights into the dynamics of these systems. Phagolysosomes containing inert
378 beads manifested distributions that met criteria for normality at most time intervals. In contrast, the
379 distribution of phagolysosomes containing dead *C. neoformans* cells initially veered away from normality
380 at 1 h but in later time intervals approached normality and met the criteria for normality at 3 h. One
381 interpretation of this result is that the process of phagocytosis is itself a randomizing system with
382 Gaussian noise resulting from resulting phagosome formation and the initial acid base reactions
383 between increasing proton flux and quenching glucuronic acids in the capsular polysaccharide [15].
384 With time, the titration was completed as dead cells did not synthesize additional polysaccharide and
385 the distribution moved toward normality. A similar effect may have occurred with strains 265, 179 and
386 the urease deficient strain. Convergence to or away from normality could reflect the sum of a myriad of
387 effects that affect phagolysosomal pH, including the intensity of acidification, the volume of the
388 phagolysosome that is determined largely by the capsule radius, the glucuronic acid composition of the
389 capsule, the production of ammonia by urease and the leakiness of the phagolysosome to cytoplasmic
390 contents with their higher pH. Although our experiments cannot sort out the contributions of these
391 factors they suggest that in combination they produce Gaussian noise effects that push or pull the
392 distribution to or from normality.

393 In this study the limitations of current experimental design forced us to measure phagolysosomal pH at
394 discrete time intervals rather than a continuous function of time. This in turn produced a more global
395 rather than a granular picture of the changing dynamics of phagolysosomal pHs. Traditional signal
396 sampling theory defines a threshold sampling frequency (the Nyquist frequency [36, 37]) above which
397 the structure of a signal can be fully captured when sampled. This frequency is defined as twice the

maximal frequency component of a function when represented, for instance, by its Fourier transform [38]. Hence, with changes in pH of an individual phagosome occurring on the order of minutes [4, 5], our sampling rate of every hour was not sufficient to capture the full structure of any one phagosome's unique course of pHs—a course that, in itself, could conceivably be characterized as stochastic or deterministic. Additionally, inherent to any act of observational measurement is an omission of the fluctuations in value that might occur over the course of taking the measurement—effectively further limiting the rate at which a system can be sampled and potentiating failure to capture the full (and true) structure of a dynamical system. With our described methods, we've instead focused our analysis on the evolution of the distribution of phagosomal pHs rather than the trajectory of any individual phagosomal pH overtime and ultimately, on the steady state to which these distributions are trending rather than nuances in their course of getting there.

Given that phagosomal pH will impact fungal growth in the phagosome [13] and the activity of many enzymes [39], the nature of the phagolysosomal pH distribution provides important insights into this system. The finding that the pH distribution for cryptococcal phagolysosomes is stochastic implies a strong role for the element of chance on the outcome of the macrophage-fungal cell interaction. This, in turn, implies an inherent unpredictability in the outcome of the struggle in each phagolysosome. Consequently, similar inputs as represented by ingestion of comparable fungal cells could have very different outputs with regards to the survival of the fungal or macrophage cells. Unpredictability at the level of the phagosome could impart unpredictability at the level of the microbe-host interaction and contribute to highly variable outcomes observed in infectious diseases. In this regard, the mean number of bacteria in phagosomes and cytoplasm of macrophages infected with the intracellular pathogen *Franciscella tularensis* exhibits stochastical dynamics [40], which in turn could result from the type of stochastic processes in phagosome formation noted here.

421 A stochastic dynamical process for phagolysosomal acidification could provide immune phagocytic cells
422 and their hosts with their best chance for controlling ingested microbes. When a phagocytic cell ingests
423 a microbe it has no information as to the pH range tolerated by the internalized microbe. For example,
424 an acidic environment favors pathogenic microbes such as *C. neoformans* [19] and *Salmonella*
425 *typhimrium* [41] whereas for *M. tuberculosis* a less acidic phagosomal pH is conducive to intracellular
426 survival [42]. During an infectious process when the immune system is confronting a large number of
427 microbial cells the random nature of the final phagosomal pH means that some fraction of the infecting
428 inoculum will be controlled by initial ingestion, possibly killed and the process of antigen presentation
429 would proceed to elicit powerful adaptive responses to control the infection. Hence, chance in
430 phagolysosomal pH acidification could allow phagocytic cells with a mechanism for hedging their bets
431 such that the stochastic nature of the process is itself a host defense mechanism.

432 In biology, bet-hedging was already described by Darwin as a strategy to overcome an unpredictable
433 environment [43], which is now known as diversified bet-hedging. That is, diversify offspring genotype
434 to ensure survival of the few, at the expense of reducing the mean inclusive fitness of the parent.
435 Scholars have now introduced two additional bet-hedging strategy. First, conservative bet-hedging,
436 where individuals use the same low-risk however successful strategy regardless of their environment.
437 Second, Adaptive bet-hedging in which individuals employ a prediction mechanism to anticipate future
438 environmental conditions. Some studies also propose that a mix of these may be used by biological
439 organisms. The main idea behind a bet-hedging strategy under the assumption of multiplicative fitness,
440 is that to maximize long-term fitness, an organism has to lower its variance in fitness between
441 generations [44-46].

442 Our observations suggest that, as a population, macrophages perform a bet-hedging strategy when
443 faced with a microbe with unknown pathogenic potential. They bet-hedge by introducing a pH level as
444 non-hospitable to pathogens as possible, while still maintaining biologically possible levels. However,

445 such an approach can select for acid-resistant microbes. Our observation suggests that to avoid an arms-
446 race, the macrophage not only lowers the pH level to a level that is unfavorable to most microbes, but
447 also introduces randomness in the achieved pH, such that ingested microbes are less likely to adapt to
448 the potentially hostile environment. To fully analyze the consequences of the strategy adopted by the
449 observed macrophages, a closer analysis is required that considers the costs and benefits provided to
450 the hosts (macrophages) while utilizing such a bet-hedging strategy. Although this is outside of the
451 scope of this current work as additional measurement to address these costs and benefits are required,
452 our observations suggest this line of investigation for future studies.

453 In summary, we document that phagosomal acidification, a critical process for phagocytic cell efficacy in
454 controlling ingested microbial cells manifests stochastic dynamics. This in turn implies a large role for
455 chance in the resolution of the conflict played out between microbes and host phagocytic cells in
456 individual phagosomes. Recently we have argued that chance is also a major determinant of individual
457 susceptibility to infectious diseases at the organismal level [47]. Chance in the outcome of infectious
458 disease outcomes in individual hosts may reflect the sum of innumerable chance events for host-
459 microbe interactions at the cellular level, which include the process of phagosome acidification.

460

461 **Acknowledgements**

462 Arturo Casadevall is supported by grants R01HL059842, 5R01AI033774, 5R37AI033142, and
463 5R01AI052733. Quigly Dragotakes is supported by a fellowship from the Achievement Rewards for
464 College Scientists (ARCS) Foundation Metro-Washington Chapter.

465

466 **REFERENCES**

1. Broderick NA. A common origin for immunity and digestion. Frontiers in immunology. 2015;6:72. Epub 2015/03/10. doi: 10.3389/fimmu.2015.00072. PubMed PMID: 25745424; PubMed Central PMCID: PMCPmc4333870.

2. Rosales C, Uribe-Querol E. Phagocytosis: A Fundamental Process in Immunity. BioMed research international. 2017;2017:9042851. Epub 2017/07/12. doi: 10.1155/2017/9042851. PubMed PMID: 28691037; PubMed Central PMCID: PMCPmc5485277.

3. Jankowski A, Scott CC, Grinstein S. Determinants of the phagosomal pH in neutrophils. The Journal of biological chemistry. 2002;277(8):6059-66. Epub 2001/12/18. doi: 10.1074/jbc.M110059200. PubMed PMID: 11744729.

4. Bouvier G, Benoliel AM, Foa C, Bongrand P. Relationship between phagosome acidification, phagosome-lysosome fusion, and mechanism of particle ingestion. Journal of leukocyte biology. 1994;55(6):729-34. Epub 1994/06/01. PubMed PMID: 8195699.

5. Geisow MJ, D'Arcy Hart P, Young MR. Temporal changes of lysosome and phagosome pH during phagolysosome formation in macrophages: studies by fluorescence spectroscopy. The Journal of cell biology. 1981;89(3):645-52. Epub 1981/06/01. PubMed PMID: 6166620; PubMed Central PMCID: PMCPmc2111800.

6. Feldmesser M, Kress Y, Novikoff P, Casadevall A. *Cryptococcus neoformans* is a facultative intracellular pathogen in murine pulmonary infection. Infect Immun. 2000;68(7):4225-37.

7. Levitz SM, Nong SH, Seetoo KF, Harrison TS, Speizer RA, Simons ER. *Cryptococcus neoformans* resides in an acidic phagolysosome of human macrophages. Infect Immun. 1999;67(2):885-90.

8. Ma H, Croudace JE, Lammas DA, May RC. Expulsion of live pathogenic yeast by macrophages. Curr Biol. 2006;16(21):2156-60.

9. Alvarez M, Casadevall A. Phagosome fusion and extrusion, and host cell survival following *Cryptococcus neoformans* phagocytosis by macrophages. Current Biology. 2006;16:2161-5.

491 10. Ma H, Croudace JE, Lammas DA, May RC. Direct cell-to-cell spread of a pathogenic yeast. BMC
492 Immunol. 2007;8:15.
493 11. Alvarez M, Casadevall A. Cell-to-cell spread and massive vacuole formation after Cryptococcus
494 neoformans infection of murine macrophages. BMC Immunol. 2007;8:16.
495 12. De Leon-Rodriguez CM, Rossi DCP, Fu MS, Dragotakes Q, Coelho C, Guerrero Ros I, et al. The
496 Outcome of the Cryptococcus neoformans-Macrophage Interaction Depends on Phagolysosomal
497 Membrane Integrity. Journal of immunology (Baltimore, Md : 1950). 2018;201(2):583-603. Epub
498 2018/06/03. doi: 10.4049/jimmunol.1700958. PubMed PMID: 29858266.
499 13. Fu MS, Coelho C, De Leon-Rodriguez CM, Rossi DCP, Camacho E, Jung EH, et al. Cryptococcus
500 neoformans urease affects the outcome of intracellular pathogenesis by modulating phagolysosomal
501 pH. PLoS Pathog. 2018;14(6):e1007144. Epub 2018/06/16. doi: 10.1371/journal.ppat.1007144. PubMed
502 PMID: 29906292; PubMed Central PMCID: PMCPmc6021110.
503 14. Freij JB, Fu MS, De Leon Rodriguez CM, Dziedzic A, Jedlicka AE, Dragotakes Q, et al. Conservation
504 of intracellular pathogenic strategy among distantly related Cryptococcal species. Infect Immun. 2018.
505 Epub 2018/05/02. doi: 10.1128/iai.00946-17. PubMed PMID: 29712729.
506 15. De Leon-Rodriguez CM, Fu MS, Corbali MO, Cordero RJB, Casadevall A. The Capsule of
507 Cryptococcus neoformans Modulates Phagosomal pH through Its Acid-Base Properties. mSphere.
508 2018;3(5). Epub 2018/10/26. doi: 10.1128/mSphere.00437-18. PubMed PMID: 30355667.
509 16. Zunino L, Soriano MC, Rosso OA. Distinguishing chaotic and stochastic dynamics from time series
510 by using a multiscale symbolic approach. Phys Rev E Stat Nonlin Soft Matter Phys. 2012;86(4 Pt
511 2):046210.
512 17. Kulp CW. Detecting chaos in irregularly sampled time series. Chaos. 2013;23(3):033110. Epub
513 2013/10/05. doi: 10.1063/1.4813865. PubMed PMID: 24089946.

514 18. Shapiro SSW, M.B. An analysis of variance test for normality (complete samples) Biometrika.
515 1965;52(3-4):591–611.
516 19. DeLeon-Rodriguez CM, Casadevall A. Cryptococcus neoformans: Tripping on Acid in the
517 Phagolysosome. Front Microbiol. 2016;7:164. Epub 2016/03/01. doi: 10.3389/fmicb.2016.00164.
518 PubMed PMID: 26925039; PubMed Central PMCID: PMCPmc4756110.
519 20. Smith LM, Dixon EF, May RC. The fungal pathogen Cryptococcus neoformans manipulates
520 macrophage phagosome maturation. Cell Microbiol. 2015;17(5):702-13. Epub 2014/11/15. doi:
521 10.1111/cmi.12394. PubMed PMID: 25394938.
522 21. Davis MJ, Eastman AJ, Qiu Y, Gregorka B, Kozel TR, Osterholzer JJ, et al. Cryptococcus
523 neoformans-induced macrophage lysosome damage crucially contributes to fungal virulence. Journal of
524 immunology (Baltimore, Md : 1950). 2015;194(5):2219-31. Epub 2015/02/01. doi:
525 10.4049/jimmunol.1402376. PubMed PMID: 25637026; PubMed Central PMCID: PMCPmc4379045.
526 22. Fierer N, Jackson RB. The diversity and biogeography of soil bacterial communities. Proceedings
527 of the National Academy of Sciences of the United States of America. 2006;103(3):626-31. Epub
528 2006/01/13. doi: 10.1073/pnas.0507535103. PubMed PMID: 16407148; PubMed Central PMCID:
529 PMCPmc1334650.
530 23. Baath E, Frostegard A, Fritze H. Soil Bacterial Biomass, Activity, Phospholipid Fatty Acid Pattern,
531 and pH Tolerance in an Area Polluted with Alkaline Dust Deposition. Appl Environ Microbiol.
532 1992;58(12):4026-31. Epub 1992/12/01. PubMed PMID: 16348828; PubMed Central PMCID:
533 PMCPmc183220.
534 24. Baath EA, K. Growth rate and response of bacterial communities to pH in limed and ash treated
535 forest soils. Soil Biol Biochem. 1994;26(8):995-1001.

536 25. Sun-Wada GH, Tabata H, Kawamura N, Aoyama M, Wada Y. Direct recruitment of H+-ATPase
537 from lysosomes for phagosomal acidification. Journal of cell science. 2009;122(Pt 14):2504-13. Epub
538 2009/06/25. doi: 10.1242/jcs.050443. PubMed PMID: 19549681.
539 26. Kinchen JM, Ravichandran KS. Phagosome maturation: going through the acid test. Nature
540 reviews Molecular cell biology. 2008;9(10):781-95. Epub 2008/09/25. doi: 10.1038/nrm2515. PubMed
541 PMID: 18813294; PubMed Central PMCID: PMCPmc2908392.
542 27. Griffiths G. On phagosome individuality and membrane signalling networks. Trends Cell Biol.
543 2004;14(7):343-51. Epub 2004/07/13. doi: 10.1016/j.tcb.2004.05.010. PubMed PMID: 15246427.
544 28. Mallik KCB, Banerjee PL, Chatterjee BD, Pramanick M. An experimental study of the course of
545 infection in mice after intranasal insufflation with *Cryptococcus neoformans*. Ind J Med Res.
546 1966;54:608-10.
547 29. Orsi CF, Colombari B, Ardizzoni A, Peppoloni S, Neglia R, Posteraro B, et al. The ABC transporter-
548 encoding gene AFR1 affects the resistance of Cryptococcus neoformans to microglia-mediated
549 antifungal activity by delaying phagosomal maturation. FEMS Yeast Res. 2009;9(2):301-10. Epub
550 2009/02/18. doi: 10.1111/j.1567-1364.2008.00470.x. PubMed PMID: 19220870.
551 30. rtavanis-Tsakonas K, Love JC, Ploegh HL, Vyas JM. Recruitment of CD63 to *Cryptococcus*
552 *neoformans* phagosomes requires acidification. Proc Natl Acad Sci U S A. 2006;103(43):15945-50.
553 31. Tucker SC, Casadevall A. Replication of *Cryptococcus neoformans* in macrophages is
554 accompanied by phagosomal permeabilization and accumulation of vesicles containing polysaccharide in
555 the cytoplasm. Proc Natl Acad Sci. 2002;99:3165-70.
556 32. Westman JM, G.;Mogavero,S.;Hube,B.;Grinstein,S. Candida al 1 bicans hyphal expansion causes
557 phagosomal membrane damage and luminal alkalinization. mBio. 2018;(in press).

558 33. Weber SM, Levitz SM. Chloroquine antagonizes the proinflammatory cytokine response to
559 opportunistic fungi by alkalizing the fungal phagolysosome. The Journal of infectious diseases.
560 2001;183(6):935-42. Epub 2001/03/10. doi: 10.1086/319259. PubMed PMID: 11237811.
561 34. Harrison TS, Griffin GE, Levitz SM. Conditional lethality of the diprotic weak bases chloroquine
562 and quinacrine against *Cryptococcus neoformans*. J Infect Dis. 2000;182(1):283-9.
563 35. Cherniak R, Valafar H, Morris LC, Valafar F. *Cryptococcus neoformans* chemotyping by
564 quantitative analysis of ^{1}H NMR spectra of glucuronoxylomannans using a computer simulated artificial
565 neural network. Clin Diagn Lab Immunol. 1998;5:146-59.
566 36. Nyquist H. Certain factors affecting telegraph speed. Bell Labs Technical Journal. 1924;3(2):324-
567 46.
568 37. Nyquist H. Certain topics in telegraph transmission theory. AIEE Trans. 1928;47:617-44.
569 38. Jerri AJ. The Shannon Sampling Theorem—Its Various Extensions and Applications: A Tutorial
570 Proceedings of the IEEE. 1977;65(11):1565-96.
571 39. Reeves EP, Lu H, Jacobs HL, Messina CG, Bolsover S, Gabella G, et al. Killing activity of
572 neutrophils is mediated through activation of proteases by K+ flux. Nature. 2002;416(6878):291-7. Epub
573 2002/03/22. doi: 10.1038/416291a. PubMed PMID: 11907569.
574 40. Gillard JJ, Laws TR, Lythe G, Molina-Paris C. Modeling early events in Francisella tularensis
575 pathogenesis. Frontiers in cellular and infection microbiology. 2014;4:169. Epub 2015/01/08. doi:
576 10.3389/fcimb.2014.00169. PubMed PMID: 25566509; PubMed Central PMCID: PMCPmc4263195.
577 41. Rathman M, Sjaastad MD, Falkow S. Acidification of phagosomes containing Salmonella
578 typhimurium in murine macrophages. Infect Immun. 1996;64(7):2765-73. Epub 1996/07/01. PubMed
579 PMID: 8698506; PubMed Central PMCID: PMCPmc174137.

580 42. Queval CJ, Brosch R, Simeone R. The Macrophage: A Disputed Fortress in the Battle against
581 Mycobacterium tuberculosis. Front Microbiol. 2017;8:2284. Epub 2017/12/09. doi:
582 10.3389/fmicb.2017.02284. PubMed PMID: 29218036; PubMed Central PMCID: PMCPmc5703847.
583 43. Darwin C. The Foundation of the Origin of Species: Two Essays Written in 1842 and 1844. .
584 Cambridge, UK: Cambridge University Press; 1909.
585 44. Slatkin M. Cascading speciation. Nature. 1974;252(5485):701-2. Epub 1974/12/20. PubMed
586 PMID: 4437620.
587 45. Philippi T, Seger J. Hedging one's evolutionary bets, revisited. Trends in ecology & evolution.
588 1989;4(2):41-4. Epub 1989/02/01. doi: 10.1016/0169-5347(89)90138-9. PubMed PMID: 21227310.
589 46. Bergman ATM. On the Natural Selection of Market Choice. Autonomous Agents and Multi-Agent
590 Systems. 2002;5(4):387-95.
591 47. Casadevall A, Pirofski LA. What Is a Host? Attributes of Individual Susceptibility. Infect Immun.
592 2018;86(2). Epub 2017/11/01. doi: 10.1128/iai.00636-17. PubMed PMID: 29084893.

593

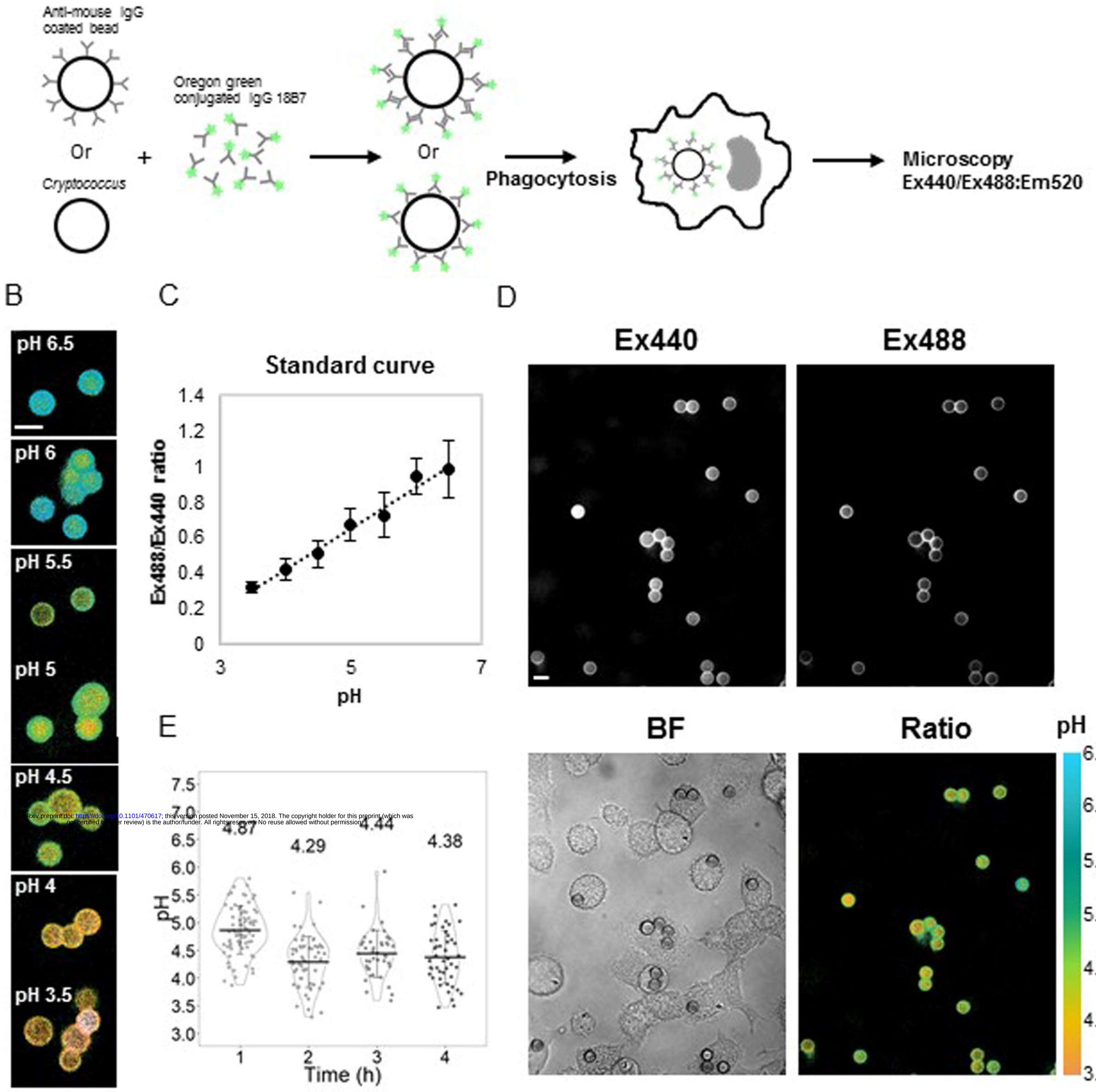

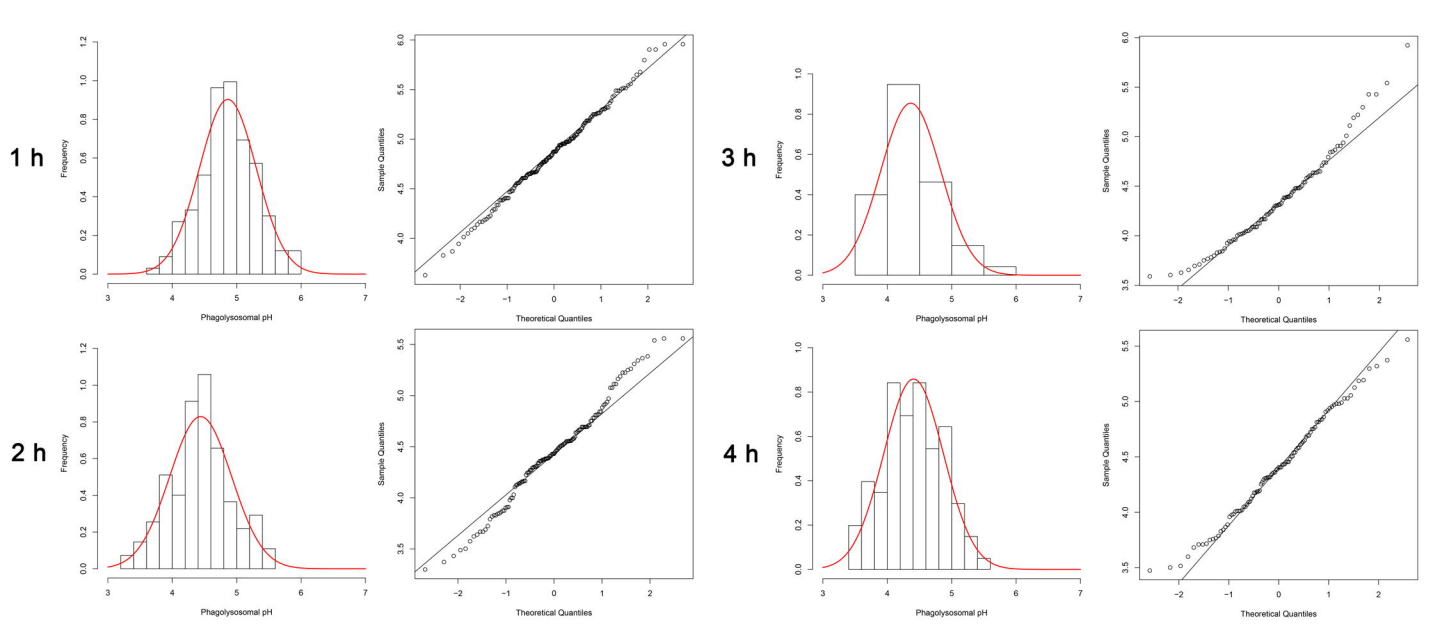
1 h
2 h
3 h
4 h
Frequency
Phagolysosomal pH
Sample Quantiles
Theoretical Quantiles

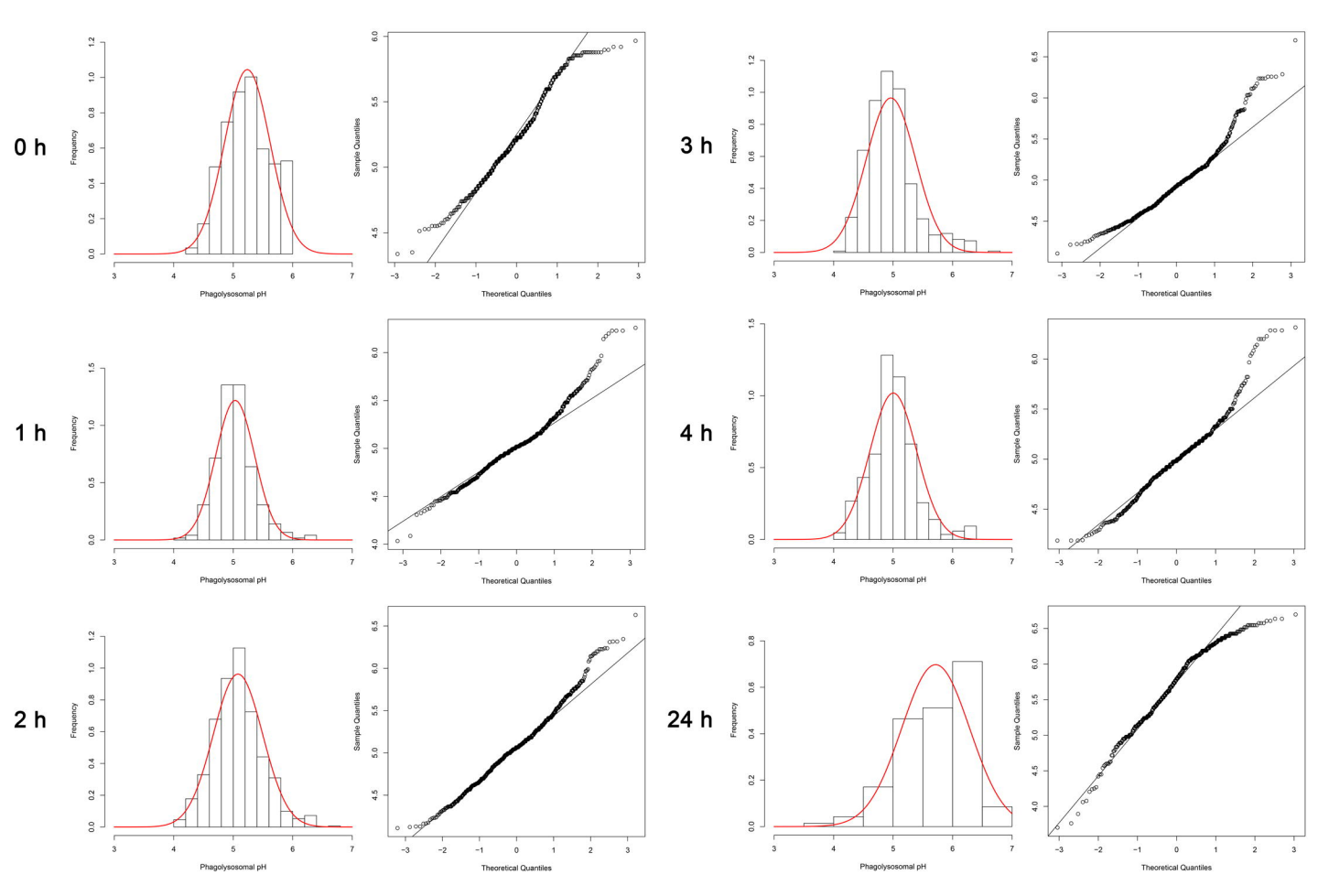
0 h
Frequency
Phagolysosomal pH
Sample Quantiles
Theoretical Quantiles
3 h
Frequency
Phagolysosomal pH
Sample Quantiles
Theoretical Quantiles
1 h
Frequency
Phagolysosomal pH
Sample Quantiles
Theoretical Quantiles
4 h
Frequency
Phagolysosomal pH
Sample Quantiles
Theoretical Quantiles
2 h
Frequency
Phagolysosomal pH
Sample Quantiles
Theoretical Quantiles
24 h
Frequency
Phagolysosomal pH
Sample Quantiles
Theoretical Quantiles

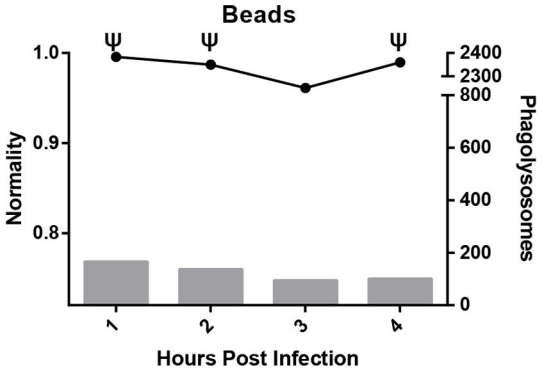
Beads
Ψ
Ψ
Ψ
Normality
1.0
0.9
0.8
Phagolysosomes
2400
2300
800
600
400
200
0
1
2
3
4
Hours Post Infection

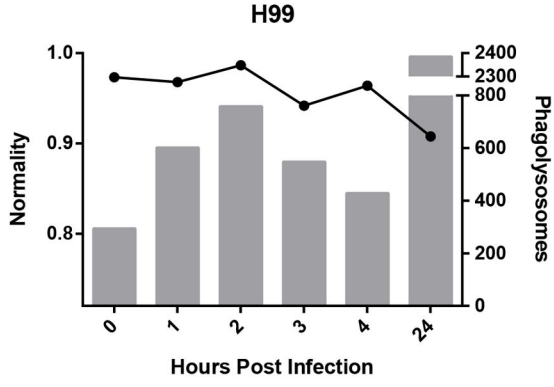
H99
Normality
1.0
0.9
0.8
Phagolysosomes
2400
2300
800
600
400
200
0
0
1
2
3
4
24
Hours Post Infection

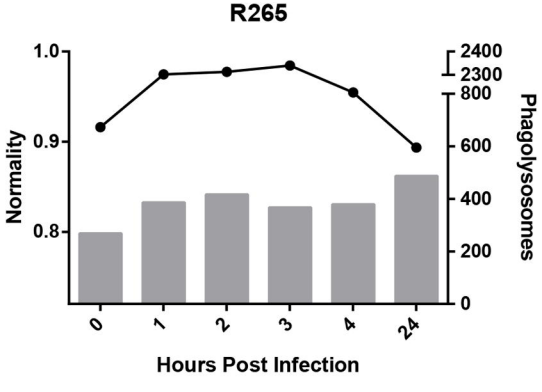
R265
Normality
1.0
0.9
0.8
Phagolysosomes
2400
2300
800
600
400
200
0
0
1
2
3
4
24
Hours Post Infection

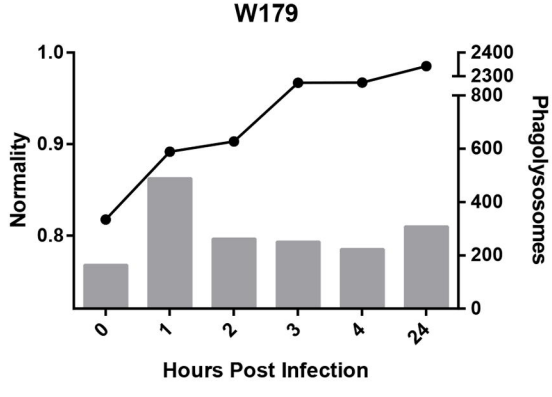
W179
Normality
1.0
0.9
0.8
Phagolysosomes
2400
2300
800
600
400
200
0
0
1
2
3
4
24
Hours Post Infection

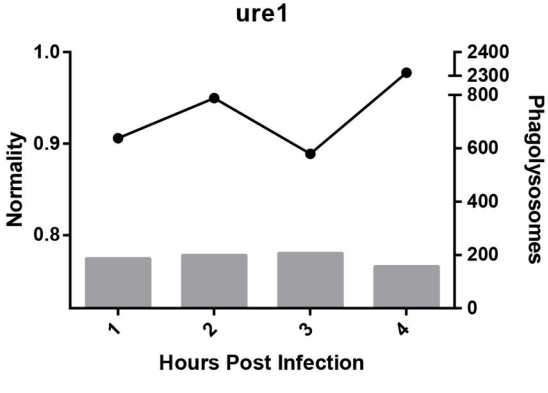
ure1
Normality
1.0
0.9
0.8
Phagolysosomes
2400
2300
800
600
400
200
0
1
2
3
4
Hours Post Infection

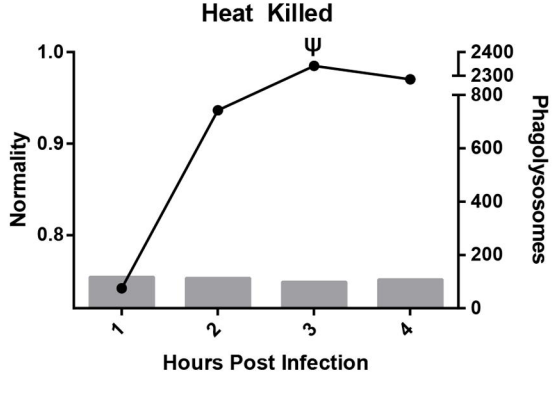
Heat Killed
Ψ
Normality
1.0
0.9
0.8
Phagolysosomes
2400
2300
800
600
400
200
0
1
2
3
4
Hours Post Infection

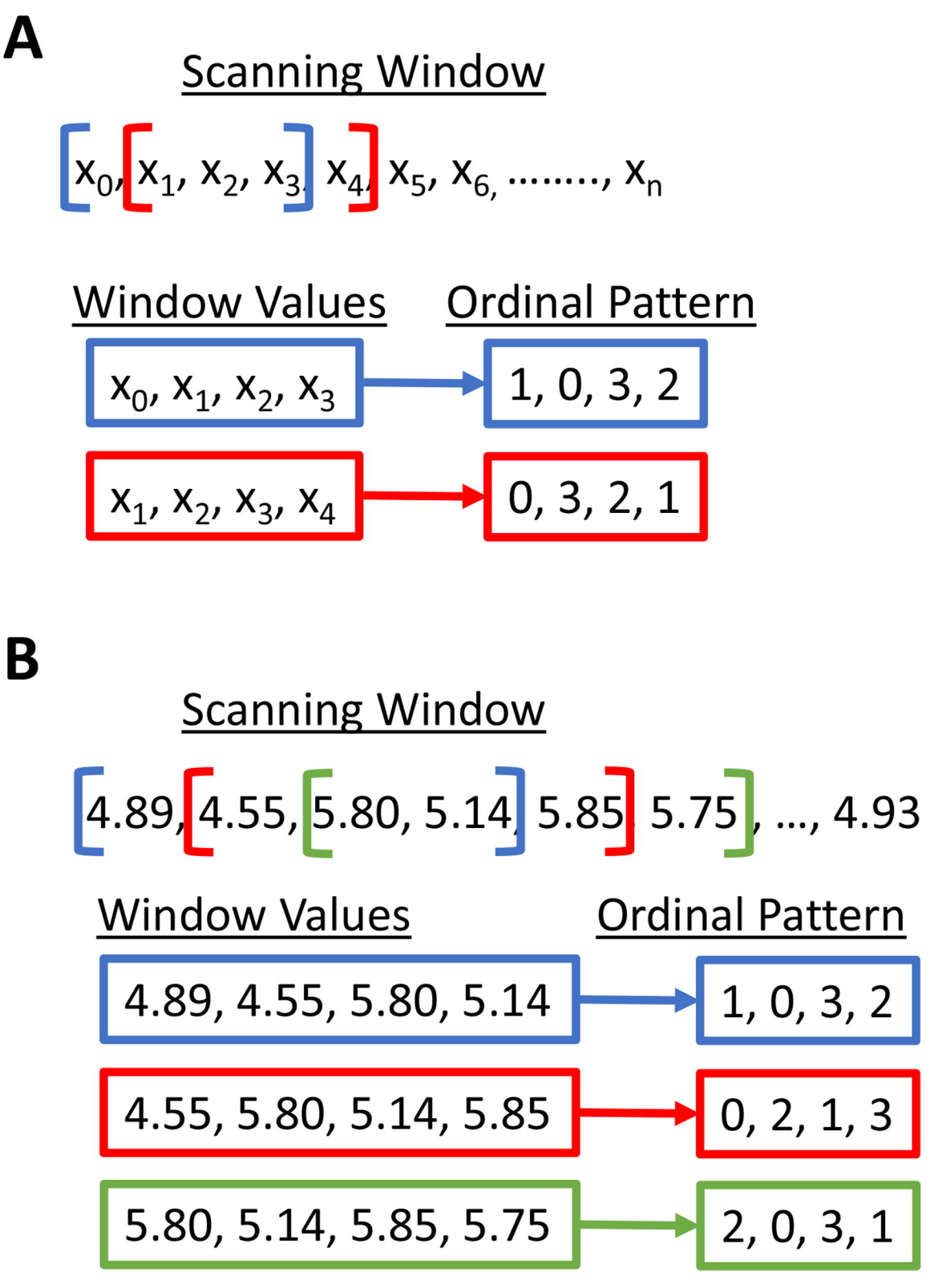
A
Scanning Window
$x_0, x_1, x_2, x_3, x_4, x_5, x_6, \ldots\ldots, x_n$
Window Values
Ordinal Pattern
x_0, x_1, x_2, x_3
1, 0, 3, 2
x_1, x_2, x_3, x_4
0, 3, 2, 1
B
Scanning Window
4.89, 4.55, 5.80, 5.14, 5.85, 5.75, …, 4.93
Window Values
Ordinal Pattern
4.89, 4.55, 5.80, 5.14
1, 0, 3, 2
4.55, 5.80, 5.14, 5.85
0, 2, 1, 3
5.80, 5.14, 5.85, 5.75
2, 0, 3, 1

1 h

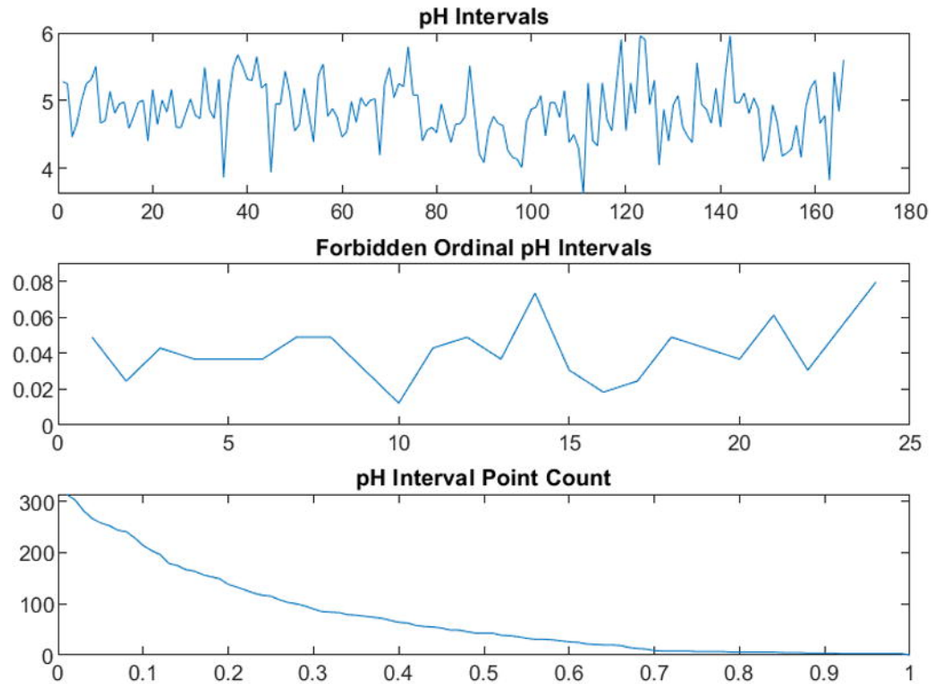
pH Intervals
Forbidden Ordinal pH Intervals
pH Interval Point Count

3 h

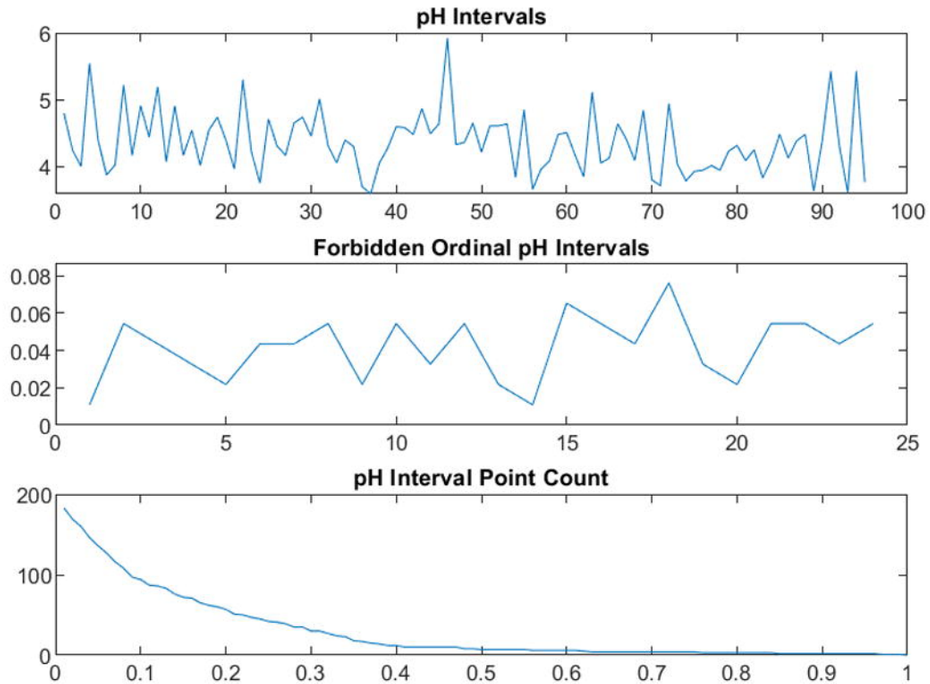
pH Intervals
Forbidden Ordinal pH Intervals
pH Interval Point Count

2 h

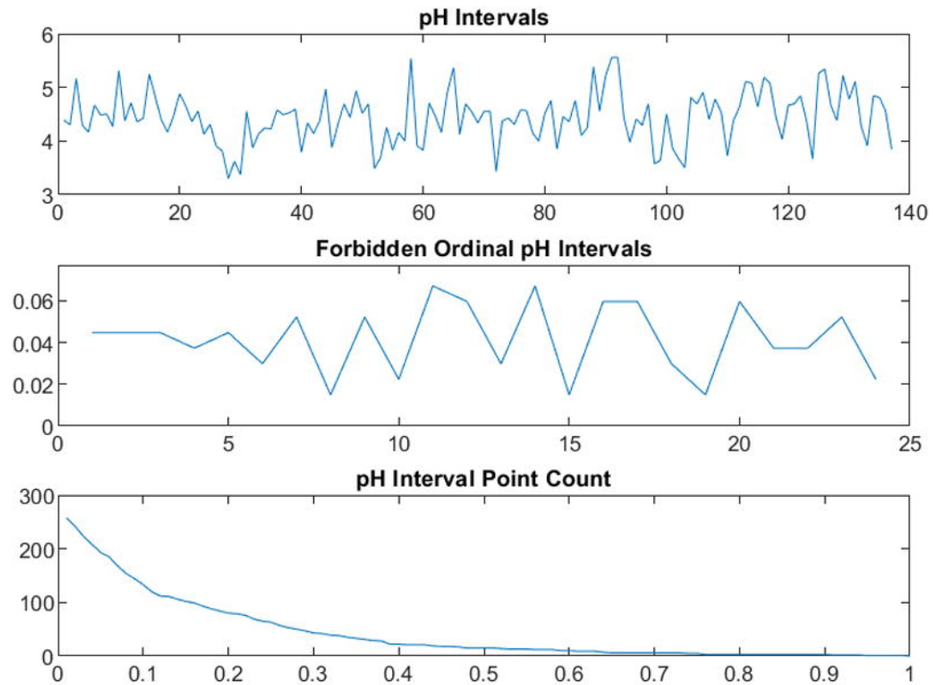
pH Intervals
Forbidden Ordinal pH Intervals
pH Interval Point Count

4 h

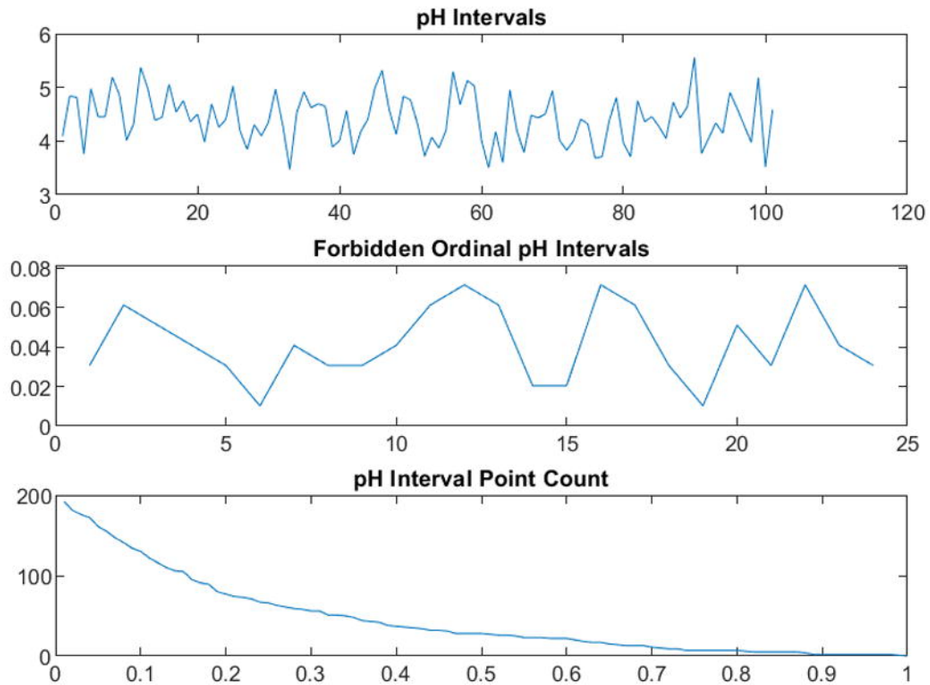
pH Intervals
Forbidden Ordinal pH Intervals
pH Interval Point Count

0 h

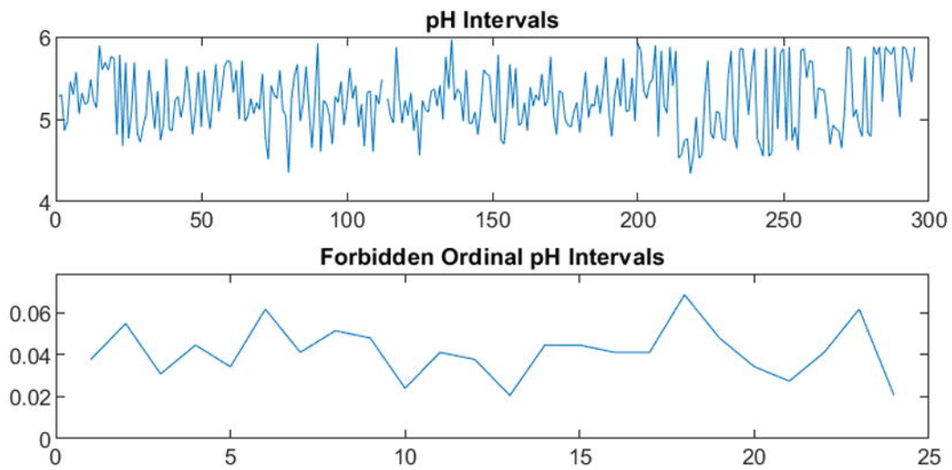

3 h

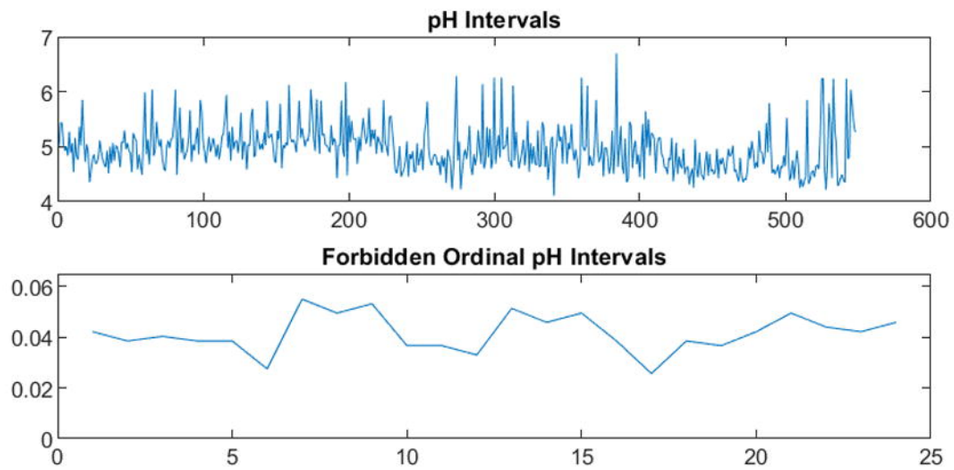

1 h

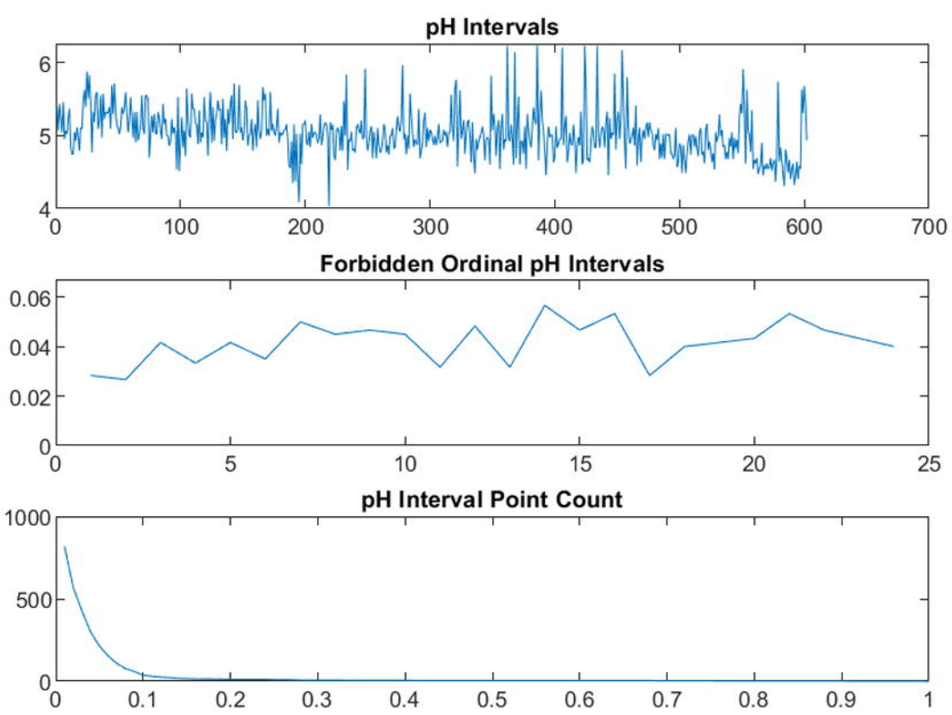

4 h

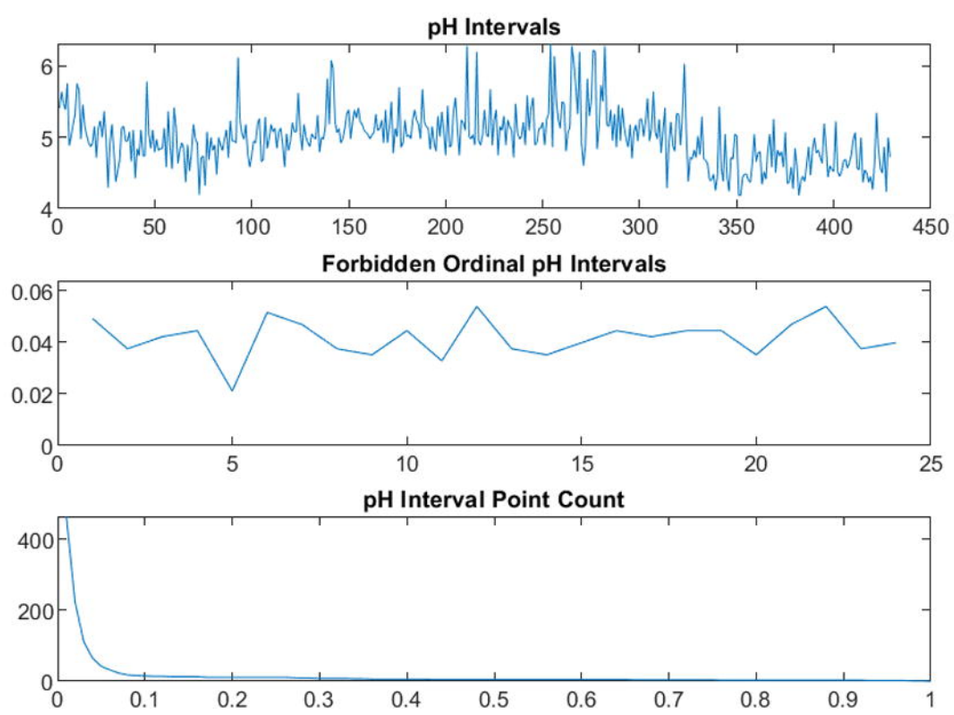

2 h

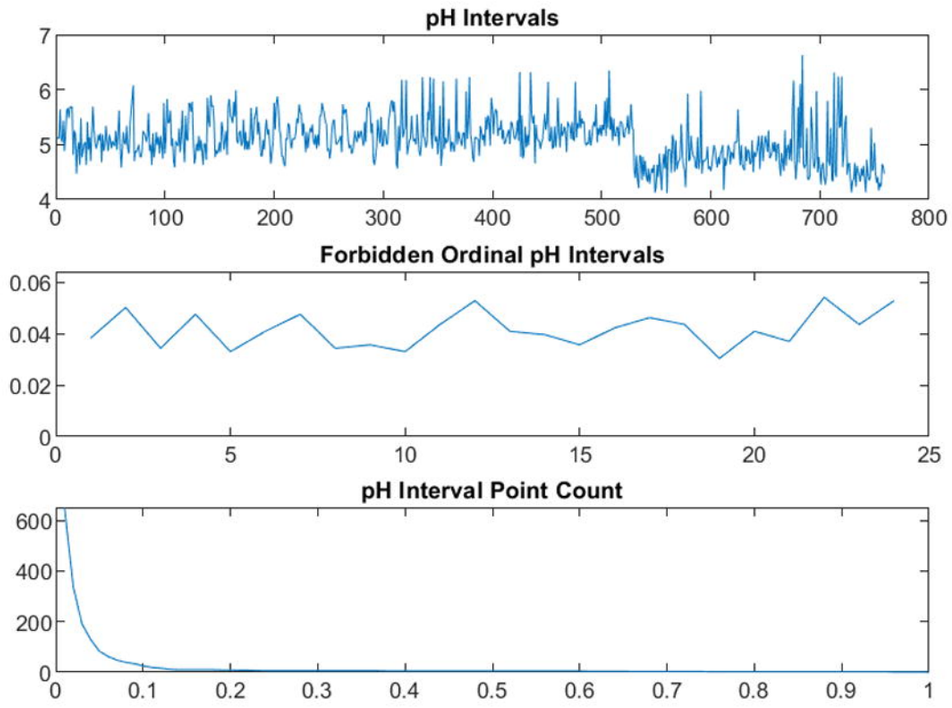

24 h

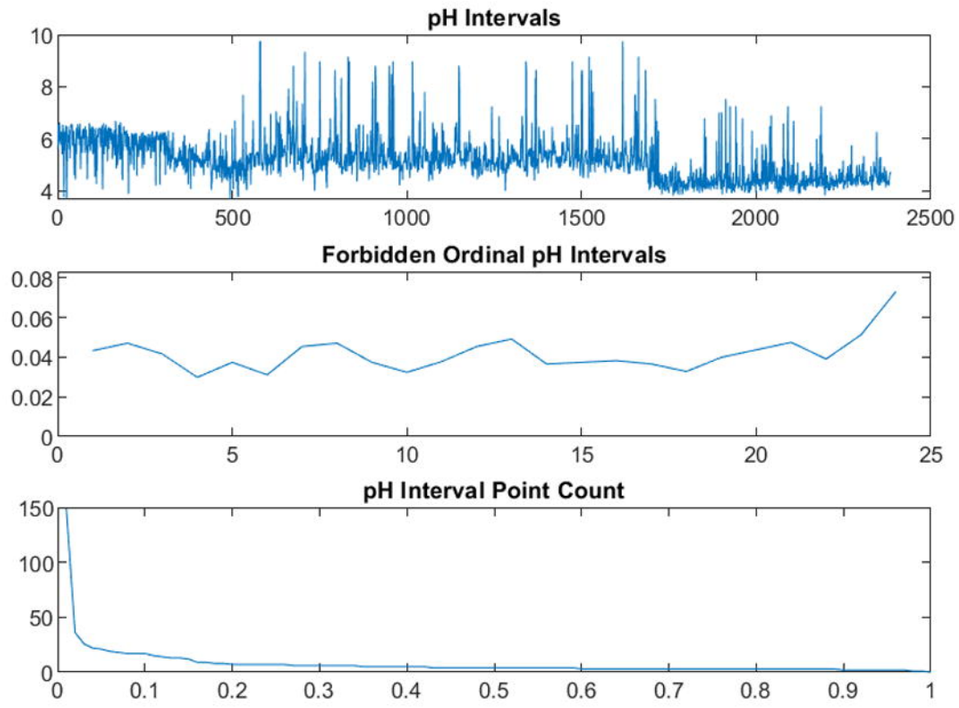

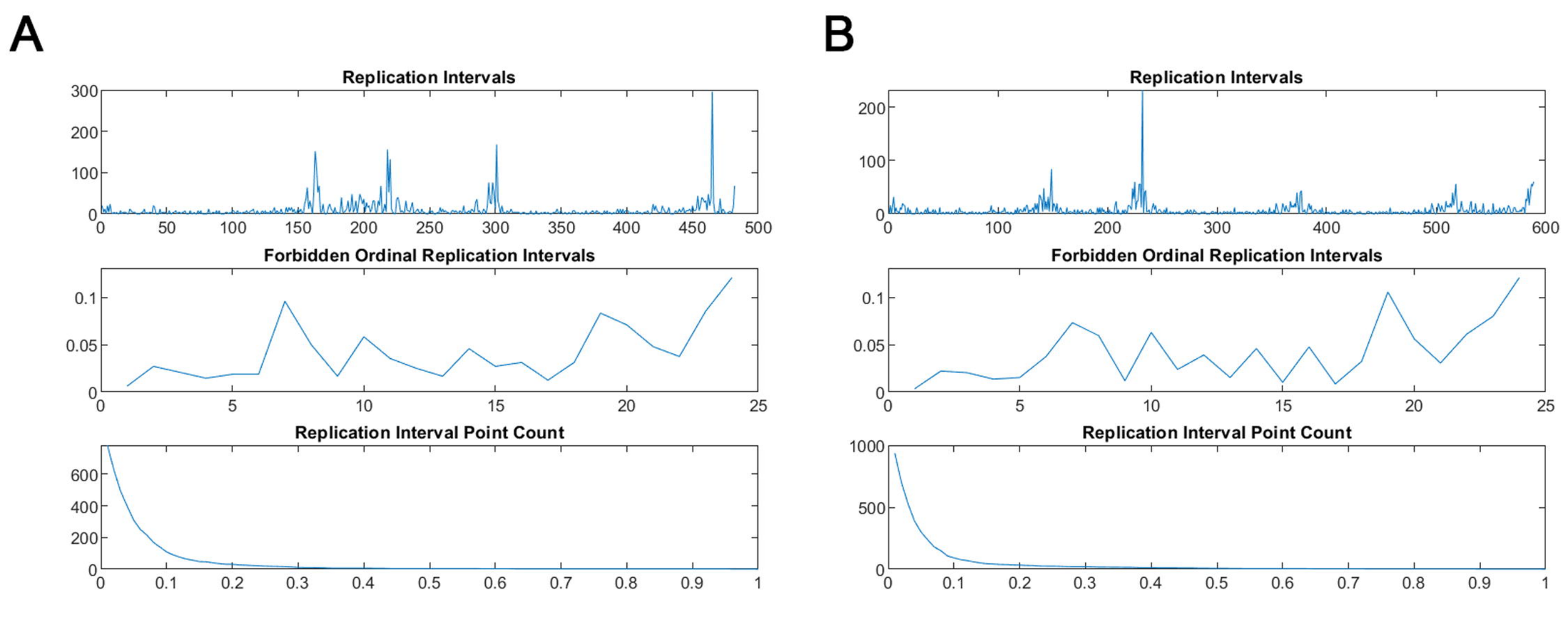
A
Replication Intervals
300
200
100
0
0 50 100 150 200 250 300 350 400 450 500
Forbidden Ordinal Replication Intervals
0.1
0.05
0
0 5 10 15 20 25
Replication Interval Point Count
600
400
200
0
0 0.1 0.2 0.3 0.4 0.5 0.6 0.7 0.8 0.9 1
B
Replication Intervals
200
100
0
0 100 200 300 400 500 600
Forbidden Ordinal Replication Intervals
0.1
0.05
0
0 5 10 15 20 25
Replication Interval Point Count
1000
500
0
0 0.1 0.2 0.3 0.4 0.5 0.6 0.7 0.8 0.9 1